Dyes and Pigments 252 (2026) 113781

Contents lists available at ScienceDirect

Dyes and Pigments

journal homepage: www.elsevier.com/locate/dyepig

Carbon-based nanopigments derived from açaí seed residues with tunable optical properties and biofunctional performance

Claudio José Reis de Carvalho [a,*], Pedro Hilton Lima Baracho [b], Francisco Dheyson de Quadro Carvalho [b], Allysson Rocha Lima [b], Antônio Matheus Osterno Leitão [c], Carlos Alberto Kenji Taniguchi [d], Adriano Lincoln Albuquerque Mattos [e], Tiago Melo Freire [b], Samuel Veloso Carneiro [b], Ralph Santos-Oliveira [f], Rafael Melo Freire [g], Pierre Basilio Almeida Fechine [b,**]

[a] Embrapa Tropical Agroindustry, Plant Physiology Laboratory, Fortaleza, CE, 60511-110, Brazil
[b] Advanced Materials Chemistry Group (GQMat), Department of Analytical and Physical Chemistry, Federal University of Ceará, Fortaleza, CE, 60451-970, Brazil
[c] Department of Statistics, Federal University of Pernambuco, Recife, PE, 50670-901, Brazil
[d] Embrapa Tropical Agroindustry, Soil Laboratory, Fortaleza, CE, 60511-110, Brazil
[e] Embrapa Tropical Agroindustry, Biomass Technology Laboratory, Fortaleza, CE, 60511-110, Brazil
[f] Brazilian Nuclear Energy Commission, Nuclear Engineering Institute, Laboratory of Nanoradiopharmacy and Synthesis of New Radiopharmaceuticals, Rio de Janeiro, 21941906, RJ, Brazil
[g] Laboratory of Nanomaterials Chemistry, Universidad Central de Chile – UCEN, Santiago, Chile

ARTICLE INFO

Keywords:
Nanopigments
Carbon quantum dot
Nanofertilizer
Biofortification
Açaí

ABSTRACT

Bio-based carbon nanomaterials have attracted increasing interest as sustainable alternatives to conventional dyes and pigments due to their tunable optical properties and multifunctionality. In this work, carbon-based nanopigments were synthesized from agro-industrial residues of açaí palm (*Euterpe oleracea*) seeds via a hydrothermal process. The resulting nanomaterials were structurally and optically characterized and evaluated for their functional performance in aqueous media and biological systems. Spectroscopic analyses revealed broad and intense absorption in the ultraviolet–visible region, associated with π–π* and n–π* electronic transitions typical of carbonaceous chromophores, along with excitation-dependent photoluminescence behaviour. Structural characterization indicated nanoscale particles with surface functional groups rich in oxygen- and nitrogen-containing moieties, which contribute to their dispersibility, optical response, and interaction with surrounding media. The nanopigments exhibited high colloidal stability and preserved their optical properties at low concentrations, demonstrating suitability for applications requiring efficient light–matter interaction. In agro-related applications, foliar treatment with the nanopigments at low concentrations (10 mg L^{-1}) promoted marked improvements in early plant development, increasing relative growth rate by 24.4% in maize and 164.6% in sorghum, while root volume increased by 23.1 and 59.9%, respectively, compared to untreated controls. These results demonstrate that the optical activity and surface functionality of the carbon nanopigments can be effectively translated into measurable biological responses, highlighting their multifunctional potential across both optically active materials and emerging agricultural technologies.

* Corresponding author.
** Corresponding author.
E-mail addresses: claudio.carvalho@embrapa.br (C.J.R. de Carvalho), phbaracho02@gmail.com (P.H.L. Baracho), dheysondequadro@hotmail.com (F.D. de Quadro Carvalho), allyssonrocha45@alu.ufc.br (A.R. Lima), matheus.osterno@ufpe.br (A.M.O. Leitão), carlos.taniguchi@embrapa.br (C.A.K. Taniguchi), adriano.mattos@embrapa.br (A.L.A. Mattos), tiagomf@ufc.br (T.M. Freire), samuel.veloso@ufc.br (S.V. Carneiro), roliveira@ien.gov.br (R. Santos-Oliveira), rafael.melo@ucentral.cl (R.M. Freire), fechine@ufc.br (P.B.A. Fechine).

https://doi.org/10.1016/j.dyepig.2026.113781
Received 9 February 2026; Received in revised form 9 April 2026; Accepted 10 April 2026
Available online 11 April 2026

1. Introduction

The açaí palm (*Euterpe oleracea* Mart.) is widely found in the estuary of the Amazon River, especially in areas of floodplains. Its fruit produces pulp that is extracted from a layer of 1-2 mm around the seed and constitutes the staple diet of traditional riverside populations [1]. Due to its nutritional properties, the pulp is widely consumed by various urban social classes both in the Amazon region and worldwide [2], encouraging cultivation of the palm outside its natural habitat in irrigated dryland environments, with annual harvests achieving yields of 6-8 tons of fruit per hectare during the adult stage [3].

Following extraction of the açaí pulp from a thin layer below the surface of the fruit, known as the pits or seeds of the açaí palm (*Euterpe oleracea* Mart.), an ample residue (700-800 kg ton^{-1} of processed fruit) is formed that is rich in residual carbon in the form of organic components and mineral nutrients. Despite studies on its small-scale use as a biochar [4], the production of bioenergy [5] or the development of composite materials, this waste generally accumulates in the urban centres of production regions and in large cities [6].

One way of using this residue, as seen with other crops, is in the production of nanofertilisers [7], which would add value to the biomass and, at the same time, return at least part of the mineral nutrients to the production areas, thereby saving on fertiliser [8–10].

Due to their small particle size, nanofertilisers are able to efficiently penetrate plant tissue [11]. This allows the nutrients to be delivered directly at the cellular level, potentially improving absorption rates compared to conventional foliar fertilisers. Due to their greater efficiency, nanofertilisers generally require smaller doses to achieve the same or better results [12]; this can reduce the costs of application and any impact on the environment. Compared to conventional fertilisers, nanofertilisers generally result in less runoff and less contamination of soils and water bodies, making them potentially more sustainable [13].

Of the nanomaterials used in agriculture, carbon-based nanoparticles show great promise. Among these, carbon dots stand out for their unique properties, such as the ability to emit fluorescence and their high biocompatibility [14], which make them ideal for applications in biotechnology and agriculture. However, the production of a fluorescent nanofertiliser from açaí seeds based on carbon dots remains unprecedented.

This study describes the processing, production, and characterisation of a nanopigment derived from açaí palm (*E. oleracea* Mart.) seed biomass after pulp extraction, which also exhibits nanofertiliser-like biofunctional activity, including toxicity assessment and growth-stimulating effects on maize and sorghum, two crops of high economic relevance.

2. Material and methods

2.1. Plant biomass

Ripe fruits of the açaí palm 'BRS-Pará' (Reg. CGEN **A7999DB**) were harvested at the Agropar Fazenda Vela Branca farm in Paracuru, Ceará, from eight-year mature plantations grown under fertigation and organic management. After harvesting, the fruits were pulped using the same process and equipment employed in all production facilities for this type of pulp [15]. The remaining pits (seeds) were washed in running water and dried for 72 h at 65 °C under ventilation. The seeds were then ground in a knife mill and passed through a 60-mesh sieve (Acai Seed Powder – ASP) at the Biomass Technology Laboratory (LTB) of Embrapa Agroindústria Tropical.

2.2. Mineral analysis

Samples of dried açaí seed powder were submitted to sulphuric digestion to determine the N, and to nitric-perchloric digestion for P, K, Ca, Mg, S, Na, B, Cu, Fe, Mn and Zn, as per procedures described in Carmo et al. (2000). A Kjeldahl distiller was used to quantify the N, while the minerals were quantified using an inductively coupled plasma optical emission spectrometer (ICP-OES) (Agilent 5100).

2.3. Synthesis of the carbon-based nanopigments

The carbon-based nanopigments, referred to here simply as carbon nanoparticles (CNP) were synthesized in the laboratory of the Advanced Materials Chemistry Group (GQMat) at the Federal University of Ceará. The chemical reagents were of analytical grade and were used without further purification. Citric acid ($C_6H_8O_7$, 99%) was purchased from the Dinâmica company, urea (CH_4N_2O, 99.5%) from NEON, and Tween® 80 ($C_{64}H_{124}O_{26}$, 65%) from Sigma-Aldrich®.

A sample of dried açaí seed powder (0.50 g) was weighed in a glass beaker, to which distilled water (50 mL) was added. The suspension was then placed in an ultrasonic bath (Solid Steel) for 15 min to facilitate water access to all powder particles. Following this, an additional volume of water (50 mL) was added to the mixture along with urea (1.00 g, 16.65 mmol) and citric acid (1.00 g, 5.20 mmol). The mixture was stirred with a magnetic stirrer at room temperature until the salts had completely dissolved, at which point it was transferred to the isostatic Teflon reactor (TFM™-PTFE).

A Berghof high-pressure reactor was used in the hydrothermal synthesis of the CNP. The aqueous samples were subjected to a heating ramp of 5 °C min^{-1} until reaching 200 °C, where they remained for 6 h with a BTC-300 controller coupled to the heating system.

After cooling, the material was centrifuged at 5000 rpm (2935 RCF) in an Eppendorf 5430 Centrifuge. The supernatant was then collected and filtered using a syringe filter with a 25 mm × 0.45 μm polyvinylidene fluoride (PVDF) membrane. Finally, the samples were dried in 5 mL Eppendorf tubes using a lyophiliser (Liobras).

2.4. Calibration curve of the synthesized CNP

Standard solutions of the lyophilised nanomaterial were prepared at the following concentrations: 0, 4, 6, 8, 10, 12, 15, 20, and 30 ppm. The absorbances of the solutions were analysed using the Cary 60 UV-Vis spectrophotometer (Agilent) and used to construct the calibration curve between the CNP concentrations and the absorbance values (Fig. 1S).

2.5. Molecular absorption spectroscopy in the ultraviolet and visible (UV-Vis) region and fluorescence spectroscopy

Absorption and fluorescence spectra of diluted CNP samples were obtained using a UV-2600 spectrophotometer and an RF-6000 spectrofluorometer (SHIMADZU). The UV-Vis spectrum was scanned in the 200-600 nm range using a 1 cm-wide glass cuvette, while for the fluorophotometer, readings were taken from 280 to 600 nm depending on the excitation wavelength – which varies from sample to sample – again using a 1 cm glass cuvette.

The fluorescence Quantum Yield (*QY*) of the nanoparticles was determined based on a procedure described previously in literature [16–18] and a solution of quinine sulfate in H_2SO_4 0.1 mol L^{-1} (QY_{ref} of 54 % at 360 nm, η = 1.33) was used as standard. The *QY* of the CNP and CNP-UAC were calculated using equation (1):

$$QY = QY_r \frac{I_s}{I_{ref}} \frac{A_{ref}}{A_s} \frac{{n_{ref}}^2}{{n_s}^2} \quad (1)$$

where *I*, *A* and *n* are the integrated emission intensity, the absorbance and the refractive index, respectively. The *s* subscript is related to the sample and *ref* is indicated to the reference. The Stockes shift was determined by the difference between the wavelength of absorbed light (excitation) and the wavelength of emitted light (fluorescence), from their respective spectra. This property corresponds to the energy band

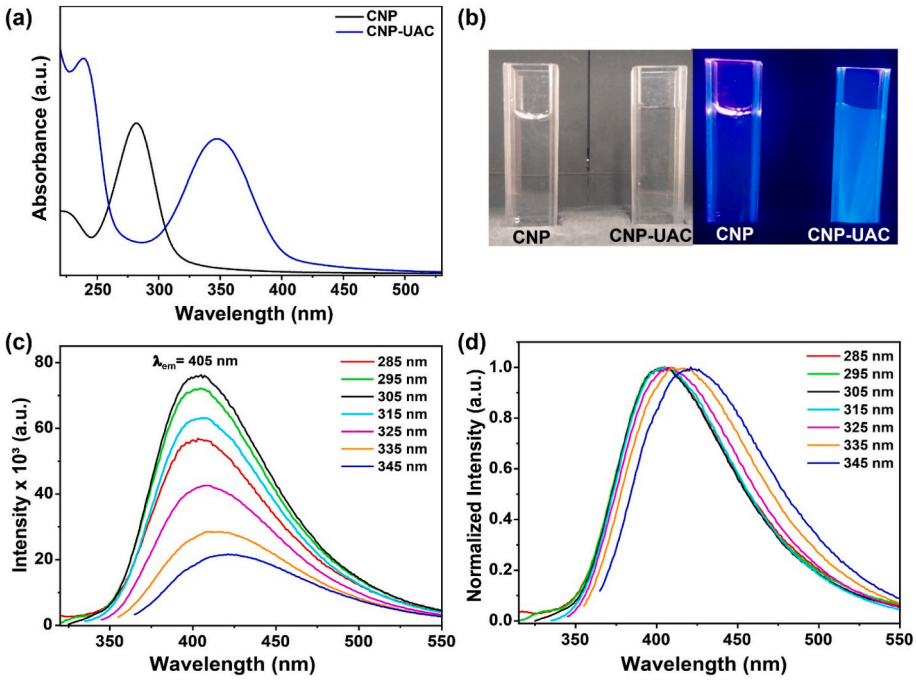

Fig. 1. Results of the molecular absorption spectroscopic analysis in the ultraviolet and visible (UV-Vis) region for the synthesized CNP: (a) UV-Vis spectra; (b) CNP and CNP-UAC samples before and after exposure to ultraviolet light; (c) Fluorescence spectra recorded in different excitation wavelengths (285 to 345 nm); (d) Normalized fluorescence spectra.

gap existing between the ground and excited states of the nanoparticles.

2.6. Fourier transform infrared absorption spectroscopy (FTIR)

The FT-IR vibrational spectra of the freeze-dried samples were obtained using a PerkinElmer FTIR/NIR Frontier spectrometer in attenuated total reflection (ATR) mode with a ZnSe crystal surface in the 4000 to 550 cm^{-1} range, running 32 scans per reading.

2.7. High-resolution transmission electron microscopy (HRTEM)

The morphology, size and distribution of the carbon nanoparticles were analysed by High-resolution transmission electron microscopy (HRTEM) using a JEOL JEM-2100 LaB6 microscope operating at an accelerating voltage of 200 kV. To prepare the samples, one drop of the diluted nanoparticle suspension was deposited on a carbon-coated copper grid and allowed to dry. The HRTEM images were obtained from different areas of the grid to ensure the representativeness of the sample.

3. Applying the nanoparticles in the maize and sorghum

3.1. Preparation of the CNP solutions

Solutions were prepared using the lyophilised CNP and distilled and deionised water at concentrations of 0, 10, 50, 100 and 150 ppm, with 0.03% v/v Tween®80 to reduce the surface tension to values close to 40 mN/m. These solutions were used for foliar application in the test plants.

3.2. Plant material

Seeds of the BRS-Gorutuba variety of maize and the 2502 variety of sorghum were used, provided by Embrapa Maize & Sorghum and Embrapa Tablelands [19,20]. Sixty rigid black plastic pots (30 for each species) were filled with approximately 2 kg of a mixture of three parts sifted soil (2 mm) collected from the surface layer (0-20 cm) at the Experimental Area in Pacajus, classified as a Red-Yellow Argisol [21], and one part coconut husk powder. The pots were lined with 1 mm polyethylene mesh to allow excess water to drain and placed on individual plastic saucers.

Four seeds were planted directly into the substrate. One week after germination, the plants were thinned leaving only the most vigorous plant in each pot. The pots were irrigated every other day with tap water until the water began to drain, receiving no additional fertiliser.

Three weeks after germination, five plants of each species were randomly selected and separated into shoots and roots. The shoots were further separated into leaves (limb to ligule) and stems, and a rectangular section, 6 cm in length, was removed from the middle of the third mature leaf. The length of the two cut edges was measured and the pieces placed in a small envelope to later estimate the ratio of weight to total leaf area. The roots were washed under running water. Both the roots and shoots were placed in separate paper bags and dried in a forced-air oven at 65 °C for 72 h. These values represent the biomass values considered at the start of treatment application.

On the day the samples were collected, the chlorophyll content in the third leaf of each plant was measured using a digital chlorophyll meter (FALKER clorofiLOG CFL 2060). The CNP solutions were then sprayed onto the leaves by means of an airbrush at a dose of 3 mL per plant. During application, the soil surface in the pots was protected by a layer of absorbent paper to prevent any liquid migrating to the roots. Five plants per species and dose were used (a total of 25 pots). The leaves were sprayed twice more at weekly intervals. One week after the third application, biomass was collected from both species, separating the shoots and roots of each plant and processing them as described above for the plants at the start of treatment application.

3.3. Growth analysis

Data on leaf dry weight after 42 days growth were used to estimate the total leaf area employing area factors. These data, together with the total plant dry weight, were used to calculate the relative growth rate (RGR) and net assimilation rate (NAR), as per equations (2) and (3) [22].

$$RGR_{(g.d^{-1})} = \frac{(ln\ W_1 - ln\ W_0)}{(t_1 - t_0)} \quad (2)$$

$$NAR_{(g.m^{-2}.d^{-1})} = \frac{(W_1 - W_0)}{(t_1 - t_0)} \cdot \frac{(ln\ S_1 - ln\ S_0)}{(S_1 - S_0)} \quad (3)$$

where:

W_0 = total biomass at the start of treatment application (t_0).
W_1 = total biomass after 15 days (t_1).
S_0 = total leaf area at the start of treatment application (t_0).
S_1 = total leaf area after 15 days (t_1).
ln = Neperian logarithm.

3.4. Determining Root Volume (RV)

The total root volume was measured using the water displacement method. Before drying, the washed roots were placed in a 250-mL measuring cylinder containing 200 mL of water. Water was then added to a level of 250 mL using a burette. The root volume was then calculated as the difference between 250 mL and the volume of water added by burette. This procedure was repeated for each sample, and the volumes recorded for later analysis.

3.5. Statistical analysis

The experiment followed a completely randomised design (CRD) with five treatments: one control and four doses of nanomaterials (10, 50, 100, and 150 ppm). Each treatment included four replications.

Analysis of variance (ANOVA) was used to identify differences between the treatments, supplemented with multiple comparison tests (Tables 1S, 2S, 3S).

4. Results and discussion

4.1. Mineral analysis of the açaí seed powder

The results of the analyses are shown in Table 1. It can be seen that the biomass of açaí seeds contains all the nutrients that are essential for plants, albeit with a significant iron content, possibly due to the richness of this element in the water used for irrigation together with the iron added during fertigation. The açaí palm (*E. oleracea*) is not considered an iron-accumulating (hyper-accumulating) species in the strict sense used in the literature on plant physiology or bioremediation [23,24], despite the species growing in floodplain environments of the Amazon River Estuary, often in alluvial soils rich in iron and organic matter [25,26].

Various studies report a moderate iron content in the fruit and seeds, ranging from 50 to 200 mg kg^{-1} dry weight, which is not high enough to classify the plant as an iron hyperaccumulator [27]. However, it is likely that the roots of the açaí palm can tolerate and absorb more iron due to their original habitat in the daily flooded alluvial zones of the Amazon River Delta [28,29], where Fe^{2+} is more bioavailable. There is, however, no consistent evidence in the literature of excessive iron storage in the shoots (leaves, stem and fruit), the results being more concentrated on the analysis of commercial pulp [30].

From a scientific point of view, the açaí palm can be considered tolerant to iron or efficient in absorbing iron under flooded conditions; it is, however, not recognised in the scientific literature as a specialist or hyper-accumulator of Fe.

Seeds typically accumulate many nutrients in the endosperm. Table 1 shows that the biomass used to synthesise the nanoparticles in this study is rich in the macro- and micronutrients necessary for plant growth and development.

Studies on the biochemical composition of this biomass also reveal a variety and abundance of lignocellulosic compounds, tannins and organic acidic sugars with more or less complex structures [31–34], which, as shown in earlier studies, can be recombined in various ways during hydrothermal synthesis and may even result in substances that stimulate plant growth [33].

Table 1 shows that the biomass used in the experiment contains significant amounts of the metals zinc (Zn), manganese (Mn) and, particularly, iron (Fe). These micronutrients, in addition to being essential for plant growth and development, are highly desirable for biofortifying fruits, tubers and forages that are grown in chemically poor tropical soils [35].

The use of biomass-derived CNP has proved effective in stimulating crop growth by stimulating photosynthesis [36,37] and in affording a greater supply of macro- and micronutrients [38,39]. As such, the use of açaí seed powder (ASP) as the basis for a nanofertiliser is quite promising, especially if applied to the production of açaí seedlings or even when included in the fertigation of commercial plantations as a way of replenishing part of the nutrients lost during commercial harvesting.

4.2. Optical and microstructural characterisation

Fig. 1A shows the spectra obtained from the synthesized samples. For the CNP sample, there is a band around 235 nm that can be attributed to the π−π* electronic transitions typical of –C═C bonds. A second band, ranging between 270 and 290 nm, is related to the n−π* transitions of –C═O bonds [40–42]. For the CNP-UAC sample, which was functionalised using urea and citric acid, a new absorption band can be seen at 347 nm. This band is characteristic of the n−π* transitions of bonds that involve functional groups on the surface of the particles, such as –NH and $–NH_2$. Fig. 1 (b) shows an image of the solutions containing the CNP and CNP-UAC samples under visible and UV light. The image reveals that the CNP sample does not exhibit fluorescence under UV light, whereas CNP-UAC shows blue fluorescence. This result, together with the band at 235 nm, suggests that açaí seed powder can be used to produce carbon nanoparticles. However, this structure lacks chromophoric groups, being mainly composed of polyaromatic structures [43,44] The observed blue fluorescence can be attributed to the presence of chromophore groups formed mainly from citric acid and urea. Thus, it should be noted that the band at 347 nm is primarily responsible for the blue fluorescence of the sample [45–47].

Carbon nanoparticles exhibited an emission band centred at 405 nm (Fig. 1C). However, a shift in the emission band towards higher wavelength regions is clearly observed in Fig. 1D. This characteristic is called bathochromic shift, since there is a tendency for light emission in the red region by the nanoparticles. This is consistent with heterogeneity of functional groups on the surface of the nanomaterials, in addition to signalling a significant variation in particle size [42,48].

The QY values for the CNP and CNP-UAC samples were 0.04% and 14.41%, respectively. The higher value for the second sample is due to the functionalization of the nanoparticle surface with amine groups, originating from urea, used as a precursor in the synthetic process. The observed Stokes shift was 154 nm and 58 nm for CNP and CNP-UAC,

Table 1
– Average values of the mineral nutrients in the açaí seed powder.

	N	P	K	Ca	Mg	S	Na	Cu	Fe	Zn	Mn	B
			g/kg						mg/kg			
Avg	6.5	0.9	5.0	0.9	0.6	0.6	0.2	5.0	240.6	24.5	11.0	14.2

Table 2
Comparison of fluorescence quantum yield (QY) values reported in the literature for carbon dots synthesized from different biomass precursors.

Biomass precursor	Synthesis method	QY (%)	Reference
Sugarcane bagasse	Hydrothermal	17.98	[52]
Biomass tar	Hydrothermal	11.3 – 27.3	[53]
Natural honey	Hydrothermal	4.19	[54]
Guava leaf extract	Green synthesis	34.0	[55]
Eggshell membrane	Hydrothermal	9.6	[56]
Hemicellulose + DES	DES-assisted synthesis	23.45	[57]
Molasses + DES	DES-assisted synthesis	50.0	[57]
Açai	Hydrothermal	**14.41**	**Present work**

Note: Only studies that explicitly reported fluorescence quantum yield (QY) values were included in this comparison. DES = deep eutectic solvent.

respectively. In this case, the functionalization of nanoparticles led to a smaller Stokes shift. This suggests reduced energy loss between excitation and emission, likely associated with a lower density of non-radiative recombination pathways. This light-converting property is crucial, as carbon dots can absorb high-energy radiation, such as UV light, and re-emit it as photosynthetically active radiation (PAR), thereby enhancing the light available for the plant's photochemical processes. Studies have shown that the quantum yield of carbon dots is a key factor in augmenting photosynthetic efficiency, with moderate yields often providing optimal enhancement of plant growth [36]. In addition, it is observed that the presence of mineral nutrients in the biomass did not significantly induce fluorescence quenching of CNP-UAC. This may be attributed to the low concentration of these nutrients during the synthesis process. The average value of 14.41% for the CNP-UAC can be considered satisfactory for nanomaterials obtained from plant biomass [49–51]. This result is attributed to synthesis parameters such as reaction time, the amount of ASP used, and the addition of a high-purity carbon source (citric acid) and a nitrogen source (urea), which collectively may have influenced the observed increase in QY. Given this QY, the material was considered suitable for application studies, for which a UV-Vis calibration curve was developed as a function of different concentrations (Fig. 1S).

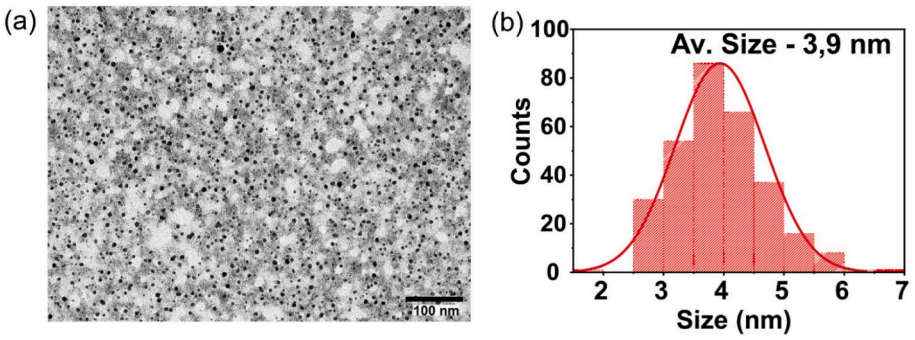

Fig. 2. (a) High-resolution transmission electron microscopy (HRTEM) image of the CNP-UAC and (b) the corresponding particle size distribution histogram, showing an average particle size.

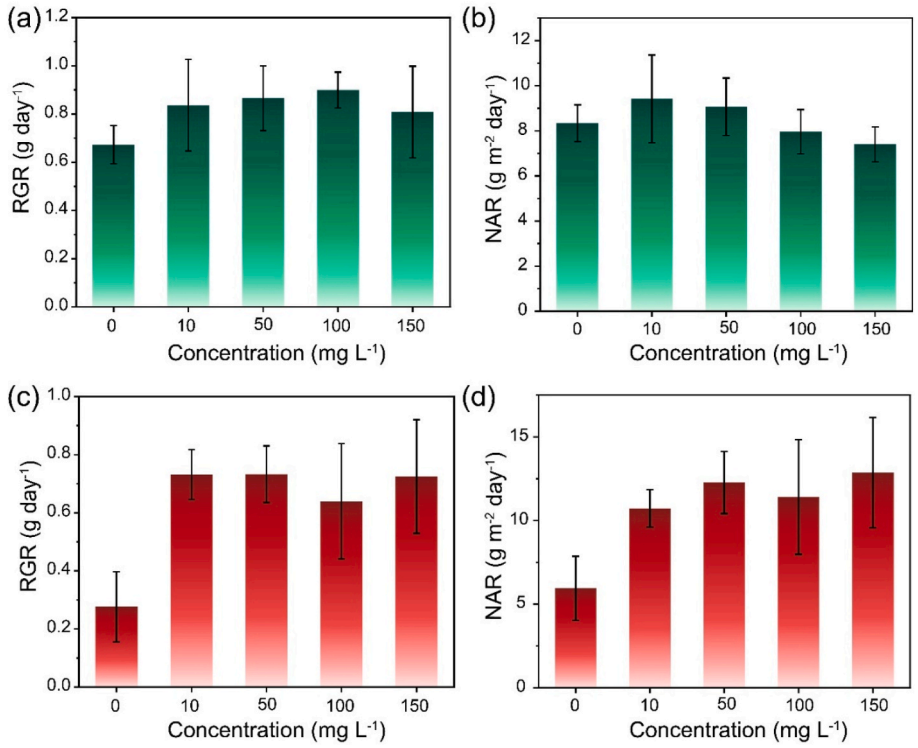

Fig. 3. Values for relative growth rate (g d^{-1}) and net assimilation rate (g m^{-2} d^{-1}) after three weekly foliar applications of nanofertiliser in maize (a and b) and sorghum (c and d).

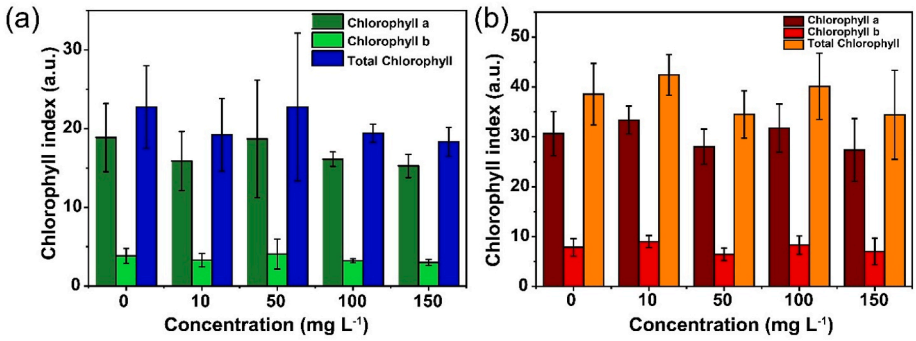

Fig. 4. Chlorophyll *a*, chlorophyll *b* and total chlorophyll in the leaf tissue of maize (a) and sorghum (b) plants after three weekly applications of nanofertiliser produced from açaí seed powder.

The roles of these substances are defined based on their chemical nature. Citric acid acts as a carbon source, necessary for the formation of the nanoparticle core, while urea corresponds to the nitrogen source, which will functionalize the surface and ensure a higher QY value.

The fluorescence quantum yield (QY) values reported for biomass-derived carbon dots are summarized in Table 2, in order to compare the optical performance of materials obtained from different precursor sources and synthesis routes. This comparison provides a useful framework for contextualizing the results obtained in the present study with respect to previously reported biomass-based carbon dots, highlighting the influence of both the precursor and the synthetic strategy on the photoluminescent properties of the nanomaterials.

To investigate the chemical structure of the samples, FTIR measurements were taken (Fig. 2S). The absorption bands in the spectra of both samples provide information about the functional groups present and the modifications induced by functionalization. The intense, broad band between 3500 and 2880 cm^{-1} is attributed to the stretching vibrations of O–H, N–H and C–H bonds. In the ACF-UAC spectrum, this band shifts and reaches its maximum around 3190 cm^{-1}, indicating the introduction of new N–H and O–H groups due to incorporation of the urea and citric acid [18,42,58]. In the CNP sample, the range between 1660 and 1600 cm^{-1} corresponds to the stretching vibrations of C═O and C═C bonds, as well as bending of the N–H bond [45]. Furthermore, in the CNP-UAC sample, the band around 1600 cm^{-1} is shifted to 1560 cm^{-1} and shows a relative increase in intensity associated with the 1660 cm^{-1} band when compared to the CNP sample. This increase can be correlated with the presence of graphitic domains, a result of the increase in C═C stretching vibrations indicating the presence of graphitic domains in the synthesized material. This characteristic is indicative of the formation of carbon quantum dots [59]. The intensification of a band around 1390 cm^{-1} in the CNP-UAC sample can be attributed to the presence of -C-N. In both samples, the band at 670 cm^{-1} corresponds to the out-of-plane folding of –C═C bonds, corroborating the existence of graphitic structures [60].

The morphology and size of the carbon nanoparticles are crucial factors that directly influence their optical properties (Fig. 2). HRTEM analysis allowed the particle size to be measured; fitting the distribution histogram with a Gaussian curve revealed an average size of 3.9 nm. The width of the curve indicates a relatively narrow distribution, suggesting the formation of nanoparticles of uniform size during synthesis. Although the histogram shows a narrow distribution, the slight variation in size, as indicated by the distribution curve and the presence of different functional groups on the surface of the CNP-UAC, explains the 'red-shift' phenomenon seen in the fluorescence spectrum. Combining these results therefore affords a comprehensive view of how the physical and chemical structure of the nanomaterial impacts its optical characteristics, confirming the effectiveness of the synthesis in the production of fluorescent nanofertilisers [60].

4.3. Effects on the growth of the maize and sorghum

Fig. 3 shows the effects of the foliar application of nanofertiliser solutions prepared in a 0.03% v/v solution of Tween®80 at concentrations of 0, 10, 50, 100 and 150 ppm on young maize and sorghum plants. The relative growth rate (RGR) indicates how the treatments affect total biomass accumulation in the plants, while the net assimilation rate (NAR) shows this effect on integrated net photosynthetic assimilation over a given period [61]. It can be seen that, in both species, the nanofertiliser achieved its maximum effect at the lowest dose (10 ppm), although the effect was greater in the sorghum. Despite there being no clear hormetic effect [62,63], there was a slight tendency for the effect of the nanofertiliser on the maize plants to decline as the concentration of the solution applied via the leaves increased, whereas in the sorghum all the treatments were superior to the control. These results show that the application of carbon quantum dots affords a consistent increase in RGR, with the effect being more evident in maize than in sorghum.

NAR values in the sorghum showed a consistent increase compared to the control with the application of carbon quantum dots. In the maize, however, the effects of the treatment were less pronounced, with the NAR remaining relatively stable at each of the concentrations under test. The stimulating effect of quantum dots is seen mainly in sorghum, while for maize, the net assimilation rate remains consistent regardless of the concentration.

Growth significantly increased in both species with only three weekly applications of the 10-ppm solution. In maize, the values for RGR and NAR were 24.36% and 13.03% higher, respectively, than the control, while in sorghum, the effects were even more noticeable, with 164.6% and 80.2%, respectively. These increases reflect the stimulation of photosynthesis, despite both species exhibiting a C4 photosynthetic pathway. The more pronounced effect observed in sorghum compared to maize may be attributed to species-specific physiological and structural differences. Sorghum has been reported to maintain higher photosynthetic stability, electron transport efficiency, and water-use efficiency under environmental stress conditions, whereas maize is more susceptible to photochemical limitations [64] Additionally, structural features such as enhanced intercellular space development and optimized gas exchange contribute to improved CO_2 diffusion and carbon assimilation in sorghum [69] TEM images showed that CNP-UAC nanopigment has an average diameter of 3.9 nm, which may facilitate the penetration into the leaf structure through stomata, cuticular cracks, or trichomes [65] Cheng et al. investigated the influence of carbon dots synthesized from biomass and observed a significant increase in photosynthesis efficiency, which was attributed to strong interaction with chloroplasts, improving light absorption and conversion [37] Thus, these characteristics suggest that sorghum can more efficiently utilize the light-converting properties of CNP-UAC, particularly under high irradiance conditions.

In contrast, there were no significant increases in the values of chlorophyll A, chlorophyll B or total chlorophyll in the leaves of either

Fig. 5. Appearance of maize (a) and sorghum (b) plants treated with three applications of nanofertiliser produced from açaí seed powder.

species (Fig. 4). As such, the increases in net assimilation rate must have been due to increased photosynthetic efficiency, but not to any increase in the levels of photosynthetic pigments.

Indeed, CNP-UAC did not affect chlorophyll content but may interact with the surface of chloroplasts due to the presence of carboxylic and amine functional groups [25,26,66]. Previous studies have shown that carbon dots can strongly associate with chloroplasts and promote electron transfer within the photosynthetic apparatus, directly influencing the light reactions of photosynthesis [67]. In addition, carbon dots can convert ultraviolet radiation into photosynthetically active radiation within chloroplasts, enhancing electron transport and photochemical efficiency without necessarily increasing chlorophyll content [36]. Thus, the observed increases in relative growth rate and net assimilation rate, in the absence of changes in chlorophyll content, indicate that the primary mechanism is not related to pigment biosynthesis but rather to enhanced photochemical efficiency. This suggests that the nanoparticles act as photophysical mediators, improving light utilization at the leaf level, a behavior often attributed to their role as nanoantennas that expand light harvesting and facilitate energy transfer processes [68]. Additionally, surface functional groups play a key role in modulating their interaction with biological systems and their optical properties [36]. Therefore, the biological responses observed in maize and sorghum can be attributed to light-driven interactions governed by nanoparticle structure and surface chemistry.

As shown in Fig. 5a and b, there was no great difference in height growth, especially in the maize plants; there was, however, an increase in vigour (stem thickness and leaf area) in both species, even at the lowest dose (10 ppm).

There was a significant increase in root volume in the plants treated with the nanofertiliser (Fig. 6). The results showed a significant effect from the level of nanofertiliser ($p = 0.002$), with no difference between the species and no interaction effects. It can be concluded that applying nanofertiliser significantly increased root growth in both species, even at low doses.

The application of nanofertiliser, even at the lowest dose (10 ppm), stimulated root production in both species, but especially in the sorghum. Each species is an important source of plant protein and the basis of animal feed in the tropics. The response obtained from the application of nanofertiliser in stimulating greater root production will definitely contribute to sustained food production in the semi-arid tropical region of both Brazil and Africa, particularly as these responses were obtained using the BRS-Gorutuba and 2502 varieties that are recommended for cultivating in these regions. It is recommended that further trials of the application of this nanofertiliser be carried out both in the field and on other types of mono- and dicotyledonous C4 and C3 crops.

5. Conclusion

Agro-industrial residues from açaí palm (*Euterpe oleracea Mart.*) seeds were successfully converted into a carbon-based nanopigment through a hydrothermal process. The synthesized nanopigment exhibited typical optical features of carbonaceous pigments, including strong ultraviolet–visible absorption and excitation-dependent photoluminescence, together with surface functional groups rich in oxygen- and nitrogen-containing moieties, which contribute to its colloidal stability and biointeraction.

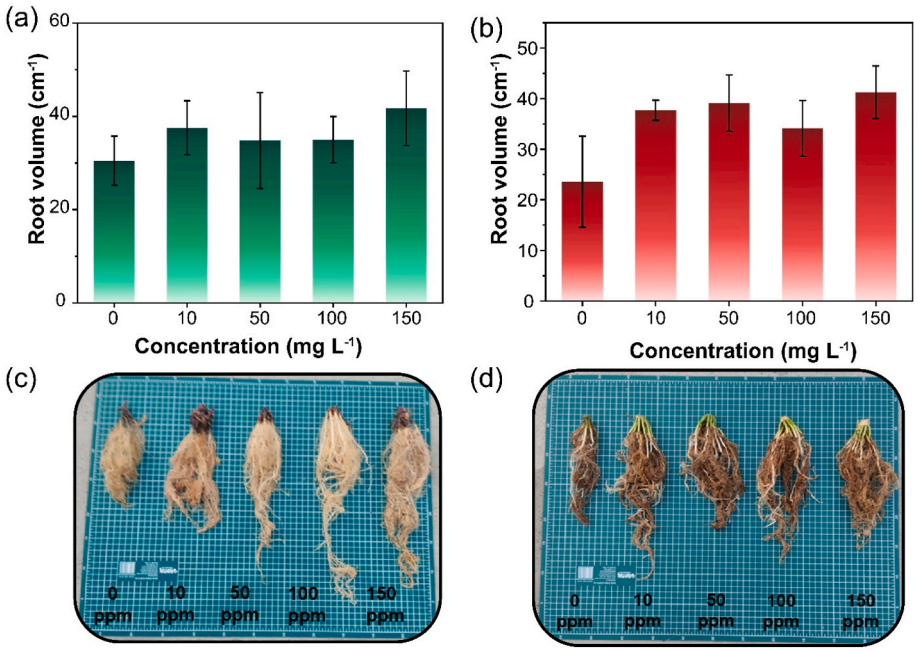

Fig. 6. Total root-system volume (mL) and representative root systems in maize (a and b) and sorghum (c and d) plants treated with three foliar applications of nanofertiliser produced from açaí seed powder.

Elemental analysis revealed significant contents of iron (Fe), manganese (Mn), and zinc (Zn), elements of agronomic relevance, particularly for crops grown in nutrient-poor tropical soils. When applied foliarly to young maize and sorghum plants, the nanopigment displayed nanofertiliser-like biofunctional activity at low concentration (10 mg L^{-1}). After three weekly applications, relative growth rate increased by 24.36% in maize and 164.6% in sorghum, while net assimilation rate increased by 13.03% and 80.2%, respectively. Root volume also increased by 23.11% in maize and 59.92% in sorghum, indicating enhanced early root system development.

These results demonstrate that açaí seed residues can be valorized into a multifunctional nanopigment combining well-defined optical properties with measurable biological effects. The material shows potential for applications beyond conventional colouring systems, including biointerfaces and agro-related technologies where pigment chemistry and biofunctional performance can be synergistically explored.

CRediT authorship contribution statement

Claudio José Reis de Carvalho: Writing – original draft, Methodology, Data curation, Conceptualization. **Pedro Hilton Lima Baracho:** Methodology, Formal analysis. **Francisco Dheyson de Quadro Carvalho:** Methodology, Formal analysis. **Allysson Rocha Lima:** Methodology, Formal analysis. **Antônio Matheus Osterno Leitão:** Validation. **Carlos Alberto Kenji Taniguchi:** Resources, Formal analysis. **Adriano Lincoln Albuquerque Mattos:** Methodology, Formal analysis. **Tiago Melo Freire:** Writing – original draft, Visualization, Conceptualization. **Samuel Veloso Carneiro:** Funding acquisition, Data curation. **Ralph Santos-Oliveira:** Funding acquisition, Data curation. **Rafael Melo Freire:** Funding acquisition, Data curation. **Pierre Basilio Almeida Fechine:** Writing – review & editing, Supervision, Project administration, Conceptualization.

Consent for publication

Not applicable.

Ethics approval and consent to participate

Not applicable.

Funding

This work was sponsored by Brazilian agencies: CAPES (Finance Code 001 - PROEX 23038.000509/2020–82) and CNPq (308452/2022–4). This work also received partial support from a Chilean funding Fondecyt 1241178.

Declaration of competing interest

The authors declare that they have no known competing financial interests or personal relationships that could have appeared to influence the work reported in this paper.

Acknowledgments

The authors would like to thank **Agropar Fazenda de Açaí Paracuru** – Ceará, Brasil, for providing the seed biomass material used in this study.

Appendix A. Supplementary data

Supplementary data to this article can be found online at https://doi.org/10.1016/j.dyepig.2026.113781.

Data availability

Data will be made available on request.

References

[1] Tavares GS, Homma AKO, Menezes AJEA, Palheta MP. Análise da produção E comercialização de açaí no estado do pará, brasil. Int J Develop Res 2020;10:35215–21.
[2] Almeida HP, Homma AKO, Menezes AJEA, Filgueiras GC, Farias Neto JT. Produção e autoconsumo de açaí pelos ribeirinhos do Município de Igarapé-Miri. Pará Res Soc Develop 2021;10:e51710918376. DOI: 0.33448/rsd-v10i9.18376.
[3] Faria Viana L, Kingo Oyama Homma A, José Elias Amorim De Menezes A, Carvalho Dos Santos J, Tomé Farias Neto J, Wagner AmanajÁs Pena H. Análise econômica do cultivo de açaizeiro (Euterpe oleracea Mart.) irrigado no nordeste paraense. Terceira Margem Amazônia 2021;7:155–69. https://doi.org/10.36882/2525-4812.2021v7i17.p155-169.
[4] Teixeira TA, Mendes FB. Valorização dos resíduos da agroindústria de beneficiamento do açaí: uma revisão. Research. Soc Develop 2023;12:e126121143799. https://doi.org/10.33448/rsd-v12i11.43799.
[5] Bufalino L, Guimarães AA, Silva BMS, Souza RLF, Melo ICNA, Oliveira DNPS, Trugilho PF. Local variability of yield and physical properties of açaí waste and improvement of its energetic attributes by separation of lignocellulosic fibers and seeds. J Renew Sustain Energy 2018;10. https://doi.org/10.1063/1.5027232.
[6] Miranda LDEVA, Mochiutti S, Cunha ACDA, Cunha HFA. Descarte e destino final de caroços de açaí na Amazônia Oriental - brasil. Ambiente & Sociedade, 25; 2022. https://doi.org/10.1590/1809-4422asoc2020138r2vu2022l2ao.
[7] Mathew S, Mathew B. A review on the synthesis, properties, and applications of biomass derived carbon dots. Inorg Chem Commun 2023;40:111223. https://doi.org/10.1016/j.inoche.2023.111223.
[8] Raliya R, Saharan V, Dimkpa C, Biswas P. Nanofertilizer for precision and sustainable agriculture : current state and future perspectives. 2018. https://doi.org/10.1021/acs.jafc.7b02178.
[9] Kaila TM, Wahiduzzaman MD, Vamsi G. Nanofertilizers in agriculture. Acta Sci Agric 2021;5:35–46.
[10] Raliya R, Fraceto LF, Mcconnell L, Li QX, Xu Y. Pioneering nano-enabled solutions for sustainable food and agriculture. ACS Agric Sci Technol 2025;5:1189–90. https://doi.org/10.1021/acsagscitech.5c00333.
[11] Chen Q, Chen L, Nie X, Man H, Guo Z, Wang X, Tu J, Jin G, Ci L. Impacts of surface chemistry of functional carbon nanodots on the plant growth. Ecotoxicol Environ Saf 2020;206:111220. https://doi.org/10.1016/j.ecoenv.2020.111220.
[12] Nekoukhou M, Fallah S, Abbasi-Surki A, Pokhrel LR, Rostamnejadi A. Improved efficacy of foliar application of zinc oxide nanoparticles on zinc biofortification, primary productivity and secondary metabolite production in dragonhead. J Clean Prod 2022;379:134803. https://doi.org/10.1016/j.jclepro.2022.134803.
[13] Sharma B, Tiwari S, Kumawat KC, Cardinale M. Nano-biofertilizers as bio-emerging strategies for sustainable agriculture development: potentiality and their limitations. Sci Total Environ 2023;860:160476. https://doi.org/10.1016/j.scitotenv.2022.160476.
[14] Dong Z, Qi J, Yue L, Zhou H, Chen L, Gu J, He Y, Wu H. Biomass-based carbon quantum dots and their agricultural applications. Plant Stress 2024;11:100411. https://doi.org/10.1016/j.stress.2024.100411.
[15] Homma AKO, NogueiraL O, Nicoli, Menezes AJEA, Carvalho JEU, Nicoli CML, Matos GB. Açaí: Novos desafios e tendências. Amazônia: Ciencia & Desenvolvimento 2006;1:7–23.
[16] Oliveira JJP, et al. Carbon quantum dots with ultra-high quantum yield for versatile turn-on sensor of gluten and cyanide ions. Dyes Pigments 2024;229:112312. https://doi.org/10.1016/j.dyepig.2024.112312.
[17] Oliveira DE, Peixoto Bruno, et al. Synthesis of luminescent chitosan-based carbon dots for Candida albicans bioimaging. Int J Biol Macromol 2023;227:805–14. https://doi.org/10.1016/j.ijbiomac.2022.12.202.
[18] Carneiro SV, Oliveira JJP, Rodrigues VSF, Fechine LMUD, Antunes RA, Neto MLA, Moura TADE, César CL, Carvalho HFDE, Paschoal AR, Freire RM, Fechine PBA. Doped carbon quantum Dots/PVA nanocomposite as a platform to sense nitrite ions in meat. ACS Appl Mater Interfaces 2022;14:43597–611. https://doi.org/10.1021/acsami.2c09197.
[19] Carvalho HWLDE, Gama EEGE, Pacheco CAP. Milho superprecoce para o semiárido. A Lavoura, 29; 2012.
[20] Guimarães MJM. Tolerância de variedades de sorgo granífero à salinidade em condições semiáridas. 100p Universidade Federal Rural de Pernambuco 2017.
[21] Lima AAC, Oliveira FNS, Aquino ARL. Classificação e Aptidão Agrícola dos Solos do Campo Experimental de Pacajus, CE, para a Agricultura. Documentos 2002;53:20.
[22] Hunt R. Basic growth analysis. Netherlands: Springer; 1990. p. 17–302p. https://doi.org/10.1007/978-94-010-9117-6. Dordrecht.
[23] Reeves RD. Tropical hyperaccumulators of metals and their potential for phytoextraction. Plant Soil 2003;249:57–65. https://doi.org/10.1023/A:1022572517197.
[24] Reeves RD. The discovery and global distribution of hyperaccumulator plants: a personal account. Ecol Res 2024;39:416–36. https://doi.org/10.1111/1440-1703.12444.
[25] Wang H-B, Liu X-P, Shu Y-C, Li G, Sun C-L, Jones DL, Zhu Y-G, Lin X-Y. Molecular composition of exogenous dissolved organic matter regulates dissimilatory iron reduction and carbon emissions in paddy soil. Environ Sci Technol 2025;59:12679–91. https://doi.org/10.1021/acs.est.5c03323.

[26] Wang Chunyan, Chen Wei, Niu Hongyang, Xu Ligang, Liu Xue. Graded nitro-engineering strategy: tuning surface states and sp2 conjugated domains of carbon quantum dots for full-color emission. Chin Chem Lett 2025;36(10):111296. https://doi.org/10.1016/j.cclet.2025.111296.
[27] Santos MM, Pasolini FS, Costa APO. Caracterização físico-química do caroço e da fibra do açaí (Euterpe oleracea mart.) via métodos clássicos e instrumentais. Brazilian J Product Eng 2023;9:143–60. https://doi.org/10.47456/bjpe.v9i2.40688.
[28] Carvalho CJR, Rombold J, Nepstad DC, Sá TD De A. Relações hidricas do açaizeiro em mata de varzea do estuario do amazonas. Rev Bras Fisiol Vegetal 1998;10:213–8.
[29] Aroni MF, Cattanio JH, Carvalho CJR De. Dynamics of greenhouse gas fluxes in açaí cultivation: comparing Amazonian upland and floodplain soils. Forests 2025;16:944. https://doi.org/10.3390/f16060944.
[30] Leão DP, Ferreira IDEJ, Nasimento OVDO, Cavalcanti V, Campelo PH, Oliveira C De MC. Bioproducts of Açaí (Euterpe spp): a review study on the composition and applications (Amazon, Brazil), 9. Research: European Academic; 2021. p. 777–95.
[31] Laurindo LF, Barbalho SM, Araújo AC, Guiguer EL, Mondal A, Bachtel G, Bishayee A Açaí. Euterpe oleracea Mart.) in health and disease: a critical review. Nutrients 2023;15:989. https://doi.org/10.3390/nu15040989.
[32] Silveira JTDA, Rosa APCDA, Morais MGDE, Victoria FN, Costa JAV. An integrative review of Açaí (Euterpe oleracea and Euterpe precatoria): traditional uses, phytochemical composition, market trends, and emerging applications. Food Res Int 2023;173:113304. https://doi.org/10.1016/j.foodres.2023.113304.
[33] Carvalho LG, Carvalho APADE, Conte-Junior CA. Bioactive compounds, antimicrobial properties of Açaí (Euterpe oleracea mart.) and its processing residues – insights for smart packaging and green chemistry. Biocatal Agric Biotechnol 2025;65:103540. https://doi.org/10.1016/j.bcab.2025.103540.
[34] Santos ÉMDOS, Toti TRB, Santos CADOS, Coco JC, Silvério LAL, Santinon C, Ataide JA, Ramos YJ, Giacon VM, Paiva-Santos AC, Fardim P, Mazzola PG. What we know about açaí by-products and topical formulations: a review. Int J Pharm 2025;680:125732. https://doi.org/10.1016/j.ijpharm.2025.125732.
[35] Morfín-Gutiérrez A, García-López JI, Ruiz-Torres NA, Álvarez-Vázquez P, Hernández-Juárez A. Small-giants in agriculture: how can nanoparticles improve cereal biofortification? Adv Agrochem 2025;4:207–16. https://doi.org/10.1016/j.aac.2025.06.003.
[36] Li Y, Xu X, Lei B, Zhuang J, Zhang X, Hu C. Magnesium-nitrogen co-doped carbon dots enhance plant growth through multifunctional regulation in photosynthesis. Chem Eng J 2021;422:130114. https://doi.org/10.1016/j.cej.2021.130114.
[37] Cheng B, Yang Z, Chen F, Yue L, Cao X, Li J, Qian HL, Yan XP, Wang C, Wang Z. Biomass-derived carbon dots with light conversion and nutrient provisioning capabilities facilitate plant photosynthesis. Sci Total Environ 2023;901:165973. https://doi.org/10.1016/j.scitotenv.2023.165973.
[38] Agnol LD, Neves RM, Maraschin M, Moura S, Ornaghi HL, Dias FTG, Bianchi O. Green synthesis of Spirulina-based carbon dots for stimulating agricultural plant growth. Sustain Mater Technol 2021;30. https://doi.org/10.1016/j.susmat.2021.e00347.
[39] Shumeyko SA, Gudkov SV. Fertilizers based on nanoparticles as sources of Macro- and microelements for plant crop growth : a review. 2024.
[40] Liu Y, Liu C, Zhang Z. Synthesis of highly luminescent graphitized carbon dots and the application in the Hg2+ detection. Appl Surf Sci 2012;263:481–5. https://doi.org/10.1016/j.apsusc.2012.09.088.
[41] Carneiro SV, Queiroz VHRDE, Cruz AAC, Fechine LMUD, Denardin JC, Freire RM, Nascimento RFDO, Fechine PBA. Sensing strategy based on carbon quantum dots obtained from riboflavin for the identification of pesticides. Sensor Actuator B Chem 2019;301:127149. https://doi.org/10.1016/j.snb.2019.127149.
[42] Jing N, Tian M, Wang Y, Zhang Y. Nitrogen-doped carbon dots synthesized from acrylic acid and ethylenediamine for simple and selective determination of cobalt ions in aqueous media. J Lumin 2019;206:169–75. https://doi.org/10.1016/j.jlumin.2018.10.059.
[43] Tiwari Santosh K, Bystrzejewski Michał, De Adhikari Amrita, Huczko Andrzej, Wang Nannan. Methods for the conversion of biomass waste into value-added carbon nanomaterials: recent progress and applications. Prog Energy Combust Sci 2022;92:101023. https://doi.org/10.1016/j.pecs.2022.101023.
[44] Tohamy Hebat-Allah S, El-Sakhawy Mohamed, Kamel Samir. A greener future: carbon nanomaterials from lignocellulose. J Renew Mater 2025;13(1):21–47. https://doi.org/10.32604/jrm.2024.058603.
[45] Liu Y, Zhang Y, Niu J, Nie L, Huang S, Liu H, Yuan S, Zhou Q. Selective fluorescent probe for sensitive determination of bisphenol A based on molecularly imprinted polymers decorated carbon dots derived from citric acid and ethylenediamine. Chemosphere 2023;324:138303. https://doi.org/10.1016/j.chemosphere.2023.138303.
[46] Zhang M, Long X, Ma Y, Wu S. Re-discussion on the essence of the ultra-bright fluorescent carbon dots synthesized by citric acid and ethylenediamine. Opt Mater 2023;135:113311. https://doi.org/10.1016/j.optmat.2022.113311.
[47] Zou W, Zhao C, Chen J, Wang Y, Jin C, Zhang X. Systematic stress persistence and recovery patterns of rice (Oryza sativa L.) roots in response to molybdenum disulfide nanosheets. Chemosphere 2023;321:138166. https://doi.org/10.1016/j.chemosphere.2023.138166.
[48] Carneiro SV, et al. Highly sensitive sensing of food additives based on fluorescent carbon quantum dots. J Photochem Photobiol Chem 2021;411:113198. https://doi.org/10.1016/j.jphotochem.2021.113198.
[49] Chang K, Zhu Q, Qi L, Guo M, Gao W, Gao Q. Synthesis and properties of nitrogen-doped carbon quantum. 2022.
[50] Yadav A, Yadav K, Abd-Elsalam K. Nanofertilizers: types, delivery and advantages in agricultural sustainability. Agrochemicals 2023;2:296–336. https://doi.org/10.3390/agrochemicals2020019.
[51] Surendran P, Lakshmanan A, Priya SS, Balakrishnan K, Rameshkumar P, Kannan K, Mahalakshmi K, Gayathri V, Vinitha G. Synthesis of fluorescent carbon quantum dots from Manihot esculenta waste peels for nonlinear optical and biological applications. Chem Phys Impact 2024;8:100515. https://doi.org/10.1016/j.chphi.2024.100515.
[52] Pandiyan Surendran, Arumugam Lakshmanan, Srirengan Sakthy Priya, Pitchan Rameshkumar, Sevugan Pushpalatha, Kannan Karthik, Pitchan Geetha, Hegde Tejaswi Ashok, Gandhirajan Vinitha. Biocompatible carbon quantum dots derived from sugarcane industrial wastes for effective nonlinear optical behavior and antimicrobial activity applications. ACS Omega 2020;5(47):30363–72. https://doi.org/10.1021/acsomega.0c03290.
[53] Deng Xiang-Yi, Feng Ya-Li, He Dong-Sheng, Zhang Zhen-Yue, Liu De-Feng, Chi Ru-An. Synthesis of functionalized carbon quantum dots as fluorescent probes for detection of Cu2+. Chin J Anal Chem 2020;48(10):e20126–33. https://doi.org/10.1016/S1872-2040(20)60054-8.
[54] Surendran P, Lakshmanan A, Priya S Sakthy, Balakrishnan K, Rameshkumar P, Kannan Karthik, Geetha P, Hegde Tejaswi Ashok, Vinitha G. Bioinspired fluorescence carbon quantum dots extracted from natural honey: efficient material for photonic and antibacterial applications. Nano-Struct Nano-Objects 2020;24:100589. https://doi.org/10.1016/j.nanoso.2020.100589.
[55] Ramanarayanan Rajita, Swaminathan Sindhu. Synthesis and characterisation of green luminescent carbon dots from guava leaf extract. Mater Today Proc 2020;33:2223–7. https://doi.org/10.1016/j.matpr.2020.03.805. *S. l.]*.
[56] Ye Zhiguo, Zhang Yanhui, Li Guixin, Li Baoxin. Fluorescent determination of Mercury(II) by green carbon quantum dots synthesized from eggshell membrane. Anal Lett 2020;53(18):2841–53. https://doi.org/10.1080/00032719.2020.1759618.
[57] Wang Yumeng, Sun Jian, He Bin, Feng Mi. Synthesis and modification of biomass derived carbon dots in ionic liquids and their application: a mini review. Green Chem Eng 2020;1(2):94–108. https://doi.org/10.1016/j.gce.2020.09.010.
[58] Ding H, Yu S-B, Wei J-S, Xiong H-M. Full-color light-emitting carbon dots with a surface-state-controlled luminescence mechanism. ACS Nano 2016;10:484–91. https://doi.org/10.1021/acsnano.5b05406.
[59] Paiva VM, Oliveira SM, Teixeira AC, Mateus JEL, Almeida CMS, Araújo JR, Costa MEHM, Suguihiro NM, D'Elia E. A new carbon quantum dot obtained from acerola (Malpighia glabra) seed waste and its application as a corrosion inhibitor of mild steel in hydrochloric acid. Biomass Bioenergy 2025;203:108264. https://doi.org/10.1016/j.biombioe.2025.108264.
[60] Swami S, Joshi A, Singh G, Rai AK, Singh SK, Singh DK. Facile synthesis and characterization of transition metal-doped carbon dots (TMDCDs) for efficient photocatalytic degradation of methylene blue. J Mol Struct 2025;1348:143467. https://doi.org/10.1016/j.molstruc.2025.143467.
[61] Poorter H. Plant growth analysis: towards a synthesis of the classical and the functional approach. Physiol Plantarum 1989;75:237–44. https://doi.org/10.1111/j.1399-3054.1989.tb06175.x.
[62] Agathokleous E, Kitao M, Calabrese EJ. Hormesis: highly generalizable and beyond laboratory. Trends Plant Sci 2020;25:1076–86. https://doi.org/10.1016/j.tplants.2020.05.006.
[63] Bondy SC. The hormesis concept : strengths and shortcomings. 2023. p. 1–10.
[64] Martínez-Goñi XS, Miranda-Apodaca J, Pérez-López U. Photosynthetic advantage without growth superiority: sorghum's paradoxical response to future climate stresses compared to maize. Environ Exp Bot 2025;237:106210. https://doi.org/10.1016/j.envexpbot.2025.106210.
[65] Dhiman VK, Rana G, Dhiman V k, Subbarayan R, Sharma M, Singh D, Jabir M, Ghotekar S, Chauhan A. Nanomaterials for sustainable agriculture: plant physiology and environmental resilience. Physiol Mol Plant Pathol 2025;139:102824. https://doi.org/10.1016/j.pmpp.2025.102824.
[66] Rishabh, Rani M, U Shanker. Advances in green carbon quantum dots: heteroatom doping strategies for pesticide detection. Food Chem 2026;514:149134. https://doi.org/10.1016/j.foodchem.2026.149134. *S. l.*.
[67] Chandra Sourov, Pradhan Saheli, Mitra Shouvik, Patra Prasun, Bhattacharya Ankita, Pramanik Panchanan, Goswami Arunava. High throughput electron transfer from carbon dots to chloroplast: a rationale of enhanced photosynthesis. Nanoscale 2014;6(7):3647–55. https://doi.org/10.1039/C3NR06079A.
[68] Guirguis A, Yang W, Conlan XA, Kong L, Cahill DM, Wang Y. Boosting plant photosynthesis with carbon dots: a critical review of performance and prospects. Small 2023;19(43):2300671. https://doi.org/10.1002/smll.202300671.
[69] Oliveira DE, Vitor Jean Paulo, Duarte Vinícius Politi, Castro DE, Mauro Evaristo, Magalhães Paulo Cesar, Pereira Fabricio José. Contrasting leaf intercellular space development in sorghum and maize modulates different tolerance capacity to water limitation. J Plant Res 2023;136(4):535–48. https://doi.org/10.1007/s10265-023-01463-7.